First Results on the Scalar WIMP-Pion Coupling, Using the XENON1T Experiment

E. Aprile,[1] J. Aalbers,[2,3] F. Agostini,[4] M. Alfonsi,[5] L. Althueser,[6] F. D. Amaro,[7] M. Anthony,[1] V. C. Antochi,[2] F. Arneodo,[8] L. Baudis,[9] B. Bauermeister,[2] M. L. Benabderrahmane,[8] T. Berger,[10] P. A. Breur,[3] A. Brown,[9] A. Brown,[3] E. Brown,[10] S. Bruenner,[11] G. Bruno,[8] R. Budnik,[12] C. Capelli,[9] J. M. R. Cardoso,[7] D. Cichon,[11] D. Coderre,[13] A. P. Colijn,[3] J. Conrad,[2] J. P. Cussonneau,[14] M. P. Decowski,[3] P. de Perio,[1] P. Di Gangi,[4] A. Di Giovanni,[8] S. Diglio,[14] A. Elykov,[13] G. Eurin,[11] J. Fei,[15] A. D. Ferella,[2] A. Fieguth,[6,*] W. Fulgione,[16,17] A. Gallo Rosso,[16] M. Galloway,[9] F. Gao,[1] M. Garbini,[4] L. Grandi,[18] Z. Greene,[1] C. Hasterok,[11] E. Hogenbirk,[3] J. Howlett,[1] M. Iacovacci,[19] R. Itay,[12] F. Joerg,[11] B. Kaminsky,[13,†] S. Kazama,[9,‡] A. Kish,[9] G. Koltman,[12] A. Kopec,[20] H. Landsman,[12] R. F. Lang,[20] L. Levinson,[12] Q. Lin,[1] S. Lindemann,[13] M. Lindner,[11] F. Lombardi,[15] J. A. M. Lopes,[7,§] E. López Fune,[21] C. Macolino,[22] J. Mahlstedt,[2] A. Manfredini,[9,12] F. Marignetti,[19] T. Marrodán Undagoitia,[11] J. Masbou,[14] D. Masson,[20] S. Mastroianni,[19] M. Messina,[8] K. Micheneau,[14] K. Miller,[18] A. Molinario,[16] K. Morå,[2,¶] M. Murra,[6] J. Naganoma,[16,23] K. Ni,[15] U. Oberlack,[5] K. Odgers,[10] B. Pelssers,[2] F. Piastra,[9] J. Pienaar,[18] V. Pizzella,[11] G. Plante,[1] R. Podviianiuk,[16] N. Priel,[12] H. Qiu,[12] D. Ramírez García,[13] S. Reichard,[9] B. Riedel,[18] A. Rizzo,[1] A. Rocchetti,[13] N. Rupp,[11] J. M. F. dos Santos,[7] G. Sartorelli,[4] N. Šarčević,[13] M. Scheibelhut,[5] S. Schindler,[5] J. Schreiner,[11] D. Schulte,[6] M. Schumann,[13] L. Scotto Lavina,[21] M. Selvi,[4] P. Shagin,[23] E. Shockley,[18] M. Silva,[7] H. Simgen,[11] C. Therreau,[14] D. Thers,[14] F. Toschi,[13] G. Trinchero,[17] C. Tunnell,[18] N. Upole,[18] M. Vargas,[6] O. Wack,[11] H. Wang,[24] Z. Wang,[16] Y. Wei,[15] C. Weinheimer,[6] D. Wenz,[5] C. Wittweg,[6] J. Wulf,[9] J. Ye,[15] Y. Zhang,[1] T. Zhu,[1] and J. P. Zopounidis[21]

(XENON Collaboration)[**]

M. Hoferichter,[25,††] P. Klos,[26,27] J. Menéndez,[28] and A. Schwenk[26,27,11]

[1]*Physics Department, Columbia University, New York, New York 10027, USA*
[2]*Oskar Klein Centre, Department of Physics, Stockholm University, AlbaNova, Stockholm SE-10691, Sweden*
[3]*Nikhef and the University of Amsterdam, Science Park, 1098XG Amsterdam, Netherlands*
[4]*Department of Physics and Astronomy, University of Bologna and INFN-Bologna, 40126 Bologna, Italy*
[5]*Institut für Physik and Exzellenzcluster PRISMA, Johannes Gutenberg-Universität Mainz, 55099 Mainz, Germany*
[6]*Institut für Kernphysik, Westfälische Wilhelms-Universität Münster, 48149 Münster, Germany*
[7]*LIBPhys, Department of Physics, University of Coimbra, 3004-516 Coimbra, Portugal*
[8]*New York University Abu Dhabi, 129188 Abu Dhabi, United Arab Emirates*
[9]*Physik-Institut, University of Zurich, 8057 Zurich, Switzerland*
[10]*Department of Physics, Applied Physics and Astronomy, Rensselaer Polytechnic Institute, Troy, New York 12180, USA*
[11]*Max-Planck-Institut für Kernphysik, 69117 Heidelberg, Germany*
[12]*Department of Particle Physics and Astrophysics, Weizmann Institute of Science, Rehovot 7610001, Israel*
[13]*Physikalisches Institut, Universität Freiburg, 79104 Freiburg, Germany*
[14]*SUBATECH, IMT Atlantique, CNRS/IN2P3, Université de Nantes, Nantes 44307, France*
[15]*Department of Physics, University of California, San Diego, California 92093, USA*
[16]*INFN-Laboratori Nazionali del Gran Sasso and Gran Sasso Science Institute, 67100 L'Aquila, Italy*
[17]*INFN-Torino and Osservatorio Astrofisico di Torino, 10125 Torino, Italy*
[18]*Department of Physics and Kavli Institute for Cosmological Physics, University of Chicago, Chicago, Illinois 60637, USA*
[19]*Department of Physics "Ettore Pancini," University of Napoli and INFN-Napoli, 80126 Napoli, Italy*
[20]*Department of Physics and Astronomy, Purdue University, West Lafayette, Indiana 47907, USA*
[21]*LPNHE, Université Pierre et Marie Curie, Université Paris Diderot, CNRS/IN2P3, Paris 75252, France*
[22]*LAL, Université Paris-Sud, CNRS/IN2P3, Université Paris-Saclay, F-91405 Orsay, France*
[23]*Department of Physics and Astronomy, Rice University, Houston, Texas 77005, USA*
[24]*Physics and Astronomy Department, University of California, Los Angeles, California 90095, USA*
[25]*Institute for Nuclear Theory, University of Washington, Seattle, Washington 98195-1550, USA*
[26]*Institut für Kernphysik, Technische Universität Darmstadt, 64289 Darmstadt, Germany*

[27]Extreme Matter Institute EMMI, GSI Helmholtzzentrum für Schwerionenforschung GmbH, 64291 Darmstadt, Germany
[28]Center for Nuclear Study, The University of Tokyo, 113-0033 Tokyo, Japan

(Received 29 November 2018; published 21 February 2019)

We present first results on the scalar coupling of weakly interacting massive particles (WIMPs) to pions from 1 t yr of exposure with the XENON1T experiment. This interaction is generated when the WIMP couples to a virtual pion exchanged between the nucleons in a nucleus. In contrast to most nonrelativistic operators, these pion-exchange currents can be coherently enhanced by the total number of nucleons and therefore may dominate in scenarios where spin-independent WIMP-nucleon interactions are suppressed. Moreover, for natural values of the couplings, they dominate over the spin-dependent channel due to their coherence in the nucleus. Using the signal model of this new WIMP-pion channel, no significant excess is found, leading to an upper limit cross section of 6.4×10^{-46} cm^2 (90% confidence level) at 30 GeV$/c^2$ WIMP mass.

DOI: 10.1103/PhysRevLett.122.071301

Introduction.—Profound evidence for the existence of dark matter has been collected throughout the past 100 years. However, its exact nature remains elusive [1,2]. A large effort is being put into the search for direct detection of weakly interacting massive particles (WIMPs), which arise as dark matter particle candidates in various theories. The search is led by dual-phase liquid xenon time projection chambers (TPCs) for masses above 5 GeV$/c^2$ [3,4]. The most sensitive experiment, XENON1T, probes spin-independent (SI) WIMP-nucleon interactions down to 4.1×10^{-47} cm^2 for 30 GeV$/c^2$ WIMP mass [5]. This limit refers to the SI isoscalar channel, which, for vanishing momentum transfer q, scales quadratically with the number of nucleons A. The SI interaction thus yields the dominant nuclear response, making it the standard search channel in the field [6–14].

In scenarios where this leading contribution vanishes or is strongly suppressed, other search channels become important. Experimentally, this aspect is addressed by dedicated analyses, e.g., for spin-dependent (SD) WIMP-nucleon interactions [15–19], nonrelativistic effective field theory (NREFT) operators [20–23], or generically q-suppressed responses [24]. Contributions beyond the widely considered SD channel include subleading NREFT operators [25–27]. In addition, a systematic expansion in the effective theory of QCD, chiral effective field theory (EFT) [28–31], valid at the relevant nuclear structure energies and momentum transfers of the order of the pion mass, reveals a new class of contributions referred to as two-body currents. These interactions proceed by the coupling of the WIMP to a virtual pion exchanged between nucleons within the nucleus. Such two-body currents that occur in the SD channel [32–34] have already had a significant impact on SD searches, improving substantially the sensitivity of xenon-based experiments to the SD WIMP-proton cross section [15–19].

In the SD channel, the inclusion of the leading two-body currents is a correction to the standard SD response, because it involves the same WIMP-nucleon coupling. However, in the SI channel the leading two-body current [35–42] cannot be absorbed into a redefinition of the WIMP-nucleon coupling. Instead, this SI two-body current involves a genuinely new combination of hadronic matrix elements and Wilson coefficients that describe the interaction of the WIMP with quarks and gluons [43]. Drawing on the analogy to both SI and SD WIMP-nucleon interactions, we demonstrate in this Letter that these new couplings can be interpreted as cross sections for a WIMP scattering off a pion, a channel that has previously not been considered in dark matter searches. For natural values of the couplings, this new WIMP-pion channel dominates over the standard SD channel due to its coherent nature. Here, we present the first results on the scalar WIMP-pion coupling based on the XENON1T experiment.

The key idea is illustrated in Fig. 1. Single-nucleon interactions, both of SI and SD nature, correspond to Fig. 1(a), where the WIMP χ interacts only with a single nucleon N within the nucleus by the exchange of a heavy

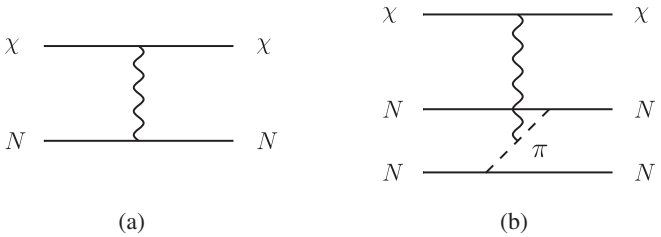

FIG. 1. Diagrams of WIMP-nucleon interactions. Solid lines refer to the WIMP (χ) and nucleon (N) fields, wavy lines to the mediating current, and the dashed line indicates the exchange of a virtual pion between two nucleons. (a) Leading WIMP coupling to one nucleon. (b) Two-nucleon contribution from the WIMP coupling to a pion-exchange current.

mediator. Integrating out the mediator produces effective operators involving the WIMP, quark, and gluon fields, which together with the hadronic matrix elements define the single-nucleon cross section that appears as a coefficient of the WIMP-nucleus rate. Corrections to this picture emerge from the fact that a nucleus is a strongly interacting many-body system, e.g., mediated by the exchange of virtual pions between two nucleons. The corresponding coupling of the WIMP through Fig. 1(b) then allows one to interpret limits from the WIMP-nucleus rate as limits on a WIMP-pion cross section. In the following, we will consider this mechanism originating from a scalar WIMP-quark coupling of the form $\bar{\chi}\chi\bar{q}q$. For additional details, see Ref. [42].

Theory.—Analyses of direct-detection experiments mostly focus on SI and SD scattering. The WIMP-nucleus cross section $d\sigma_{\chi\mathcal{N}}/dq^2$, where $\mathcal{N}$ indicates the entire nucleus, depends on the relative velocity of the WIMP in the lab-frame v and the nuclear spin J. With nuclear structure factors that encode the response of the nucleus to the interaction with WIMPs denoted by $\mathcal{F}_{\pm}^{M}$ [26] and S_{ij} [44] for SI and SD scattering, respectively, this leads to the usual decomposition [44,45]

$$\frac{d\sigma_{\chi\mathcal{N}}}{dq^2} = \frac{1}{4\pi v^2}|c_+^M\mathcal{F}_+^M(q^2) + c_-^M\mathcal{F}_-^M(q^2)|^2 + \frac{1}{v^2(2J+1)}\Big[|a_+|^2 S_{00}(q^2) + \mathrm{Re}(a_+a_-^*)S_{01}(q^2) + |a_-|^2 S_{11}(q^2)\Big]. \quad (1)$$

Even though the dependence on q itself contains valuable hints for the nature of the underlying interaction [46], the information about physics beyond the standard model (BSM) is fully encoded in the coefficients $c_{\pm}^M$ and $a_{\pm}$. They include both the coupling of the WIMP to quarks and gluons (Wilson coefficients) and the hadronic matrix elements that reflect that quarks and gluons are embedded into nucleons. The + (−) subscript indicates a same- (opposite-) sign or isoscalar (isovector) coupling for neutrons and protons. In SD scattering, it is useful to take $a_+ = a_-$, which describes the WIMP coupling to a proton, or $a_+ = -a_-$ for the coupling to a neutron.

Most analyses consider the following scenarios. First, they assume purely isoscalar SI interactions ($c_-^M = a_{\pm} = 0$), with the WIMP-nucleus cross section expressed in terms of the SI cross section off a single nucleon $\sigma_{\chi N}^{\mathrm{SI}}$,

$$\frac{d\sigma_{\chi\mathcal{N}}}{dq^2} = \frac{\sigma_{\chi N}^{\mathrm{SI}}}{4\mu_N^2 v^2}|\mathcal{F}_+^M(q^2)|^2, \qquad \sigma_{\chi N}^{\mathrm{SI}} = \frac{\mu_N^2}{\pi}|c_+^M|^2, \quad (2)$$

where μ_N is the WIMP-nucleon reduced mass. The nuclear structure factor $\mathcal{F}_+^M$ is often approximated by a Helm form factor [47], but more sophisticated nuclear calculations are available [48]. Second, one takes a purely SD coupling ($c_{\pm}^M = 0$) with $a_+ = a_-$ or $a_+ = -a_-$ written in terms of the SD cross section off a single proton or neutron $\sigma_{\chi N}^{\mathrm{SD}}$,

$$\frac{d\sigma_{\chi\mathcal{N}}}{dq^2} = \frac{\sigma_{\chi N}^{\mathrm{SD}}}{3\mu_N^2 v^2}\frac{\pi}{2J+1}S_N(q^2), \quad \sigma_{\chi N}^{\mathrm{SD}} = \frac{3\mu_N^2}{\pi}|a_+|^2, \quad (3)$$

where single nucleons are denoted by $N = \{p, n\}$ and $S_{p/n}(q^2) = S_{00}(q^2) \pm S_{01}(q^2) + S_{11}(q^2)$. Out of these scenarios, the SI response is dominant because all A nucleons contribute coherently: $\mathcal{F}_+^M(0)^2 = A^2$, with $A \sim 130$ for xenon. In contrast, in the SD channel the response does not scale with A: $[4\pi/(2J+1)]S_N(0) \sim [4(J+1)/J]\langle \mathbf{S}_N\rangle^2 = \mathcal{O}(1)$ (for nuclei with unpaired nucleons), with $\langle \mathbf{S}_{p/n}\rangle$ proton or neutron spin-expectation values of the nuclear target. (This estimate does not include contributions from two-body currents to SD scattering, which are quantitatively significant especially for the paired species [32,33], but they do not enter coherently.) Therefore, SD limits become most relevant if the SI interactions are either absent or strongly suppressed [49]. In practice, the consideration of limits on $\sigma_{\chi N}^{\mathrm{SI}}$, $\sigma_{\chi p}^{\mathrm{SD}}$, and $\sigma_{\chi n}^{\mathrm{SD}}$ corresponds to a set of slices through the BSM parameter space, which is not a complete or unique choice. For instance, one could also consider proton- or neutron-only SI cross sections ($c_+^M = \pm c_-^M$, $a_{\pm} = 0$), which are related to isospin-violating dark matter [36,50–53].

In this Letter, we consider the leading contribution beyond SI and SD scattering given in Eqs. (2) and (3). For that purpose we use chiral EFT [37], which allows one to derive a more complete set of possible WIMP interactions with nuclei. When the relevant momentum transfers are of the order of the pion mass $q \lesssim M_\pi$, such as in direct-detection experiments, chiral EFT predicts that pions, in addition to nucleons, emerge as relevant degrees of freedom. In fact, in chiral EFT, nuclear forces are mediated by pion exchanges, and also the interactions of nuclei with external probes can occur via the coupling to a pion exchanged between two nucleons. Such pion-exchange currents are very well established in electromagnetic and weak interactions in nuclei (see, e.g., Refs. [31,54]).

A chiral EFT study of WIMP interactions with nucleons indicates that pion-exchange currents [see Fig. 1(b)] enter at the same order in the chiral EFT power counting as momentum-suppressed single-nucleon currents [37]. The importance of pion-exchange currents has been stressed for SD scattering [32,33], where they lift the strict separation between proton- or neutron-only couplings. By probing the neutrons even for $a_+ = a_-$ they dramatically increase the sensitivity to $\sigma_{\chi p}^{\mathrm{SD}}$ for an experimental target, such as xenon, with an even number of (mainly paired) protons [15–19]. Similarly, pion-exchange currents constitute the most important coherent correction [38,42]. Therefore, a minimal extension of Eq. (1) adds a term corresponding to the WIMP-pion coupling, with a new combination of Wilson coefficients and hadronic matrix elements c_π, together with a novel nuclear structure factor $\mathcal{F}_\pi(q^2)$,

$$\frac{d\sigma_{\chi\mathcal{N}}}{dq^2} = \frac{1}{4\pi v^2}|c_+^M\mathcal{F}_+^M(q^2) + c_-^M\mathcal{F}_-^M(q^2) + c_\pi\mathcal{F}_\pi(q^2)|^2, \tag{4}$$

without changing the SD interactions. The decomposition in Eq. (4) suggests to consider, in addition to standard SI and SD analyses, the scenario where $c_\pm^M = a_\pm = 0$, leading to

$$\frac{d\sigma_{\chi\mathcal{N}}}{dq^2} = \frac{\sigma_{\chi\pi}^{\text{scalar}}}{\mu_\pi^2 v^2}|\mathcal{F}_\pi(q^2)|^2, \qquad \sigma_{\chi\pi}^{\text{scalar}} = \frac{\mu_\pi^2}{4\pi}|c_\pi|^2, \tag{5}$$

with scalar WIMP-pion cross section $\sigma_{\chi\pi}^{\text{scalar}}$ and WIMP-pion reduced mass μ_π. In analogy to SI and SD limits, the structure factor $\mathcal{F}_\pi$ then allows one to derive limits for $\sigma_{\chi\pi}^{\text{scalar}}$ as a function of the WIMP mass m_χ. The corresponding exclusion plot represents another slice in the BSM parameter space. It becomes relevant for regions where cancellations occur in the leading SI coupling to nucleons, e.g., in heavy-WIMP EFT [55] or so-called blind spots in the minimal supersymmetric standard model [56–58]. More general cases, e.g., retaining a nonvanishing c_+^M as well, are straightforward to consider, but the corresponding limits cannot be represented in terms of a single-particle cross section anymore.

In terms of sensitivity to single-particle cross sections, the coupling to the pion is subleading in chiral EFT with respect to SI, but dominant over SD scattering. For typical nuclear targets with $A \sim 100$ nucleons, one finds

$$A^2 \gg 4\left(\frac{M_\pi}{\Lambda_\chi}\right)^6\left(\frac{m_N}{M_\pi}\right)^2 A^2 \gg \frac{4}{3}\frac{J+1}{J}\langle \mathbf{S}_{n/p}\rangle^2, \tag{6}$$

where the middle estimate is for the WIMP-pion coupling, $\Lambda_\chi \sim 500$–600 MeV is the chiral EFT breakdown scale, and m_N is the nucleon mass. The factor $(M_\pi/\Lambda_\chi)^6$ is due to the subleading Q^3 nature of two-body currents entering quadratically in the cross section—Q is the chiral EFT expansion parameter. For the two xenon isotopes with nonvanishing spin, the above scaling is well reflected by the actual hierarchy of the structure factors: $1.7 \times 10^4 \gg 1.1 \times 10^3 \gg 0.34, 0.13$ for ^{129,131}Xe, respectively [33,38,42]. In this hierarchy, additional contributions from NREFT operators are further suppressed, because they either vanish at $q = 0$ or scale with the very small WIMP velocities $v^2 \sim 10^{-6}$ [38,42]. We stress that the scaling (6) refers to the nuclear responses only, so that this hierarchy can always be overcome by a corresponding tuning of the BSM couplings. In particular, SD [15–19] searches probe another complementary slice of the BSM parameter space corresponding to models where SI and WIMP-pion interactions vanish or are strongly suppressed.

In order to perform the transition from Eq. (2) to Eq. (5), the signal model has to be adjusted accordingly. For a given WIMP mass, it is derived from the differential recoil spectrum dR/dE_r. Accounting for the different kinematic factors in Eq. (5), the spectrum for the WIMP-pion coupling can be written as

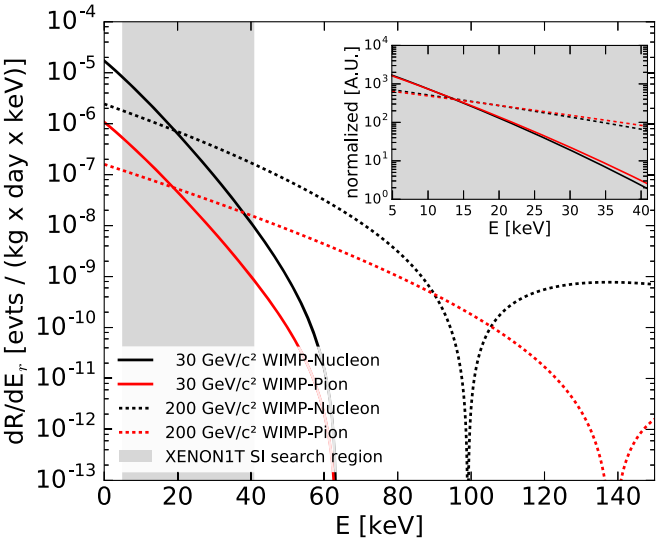

FIG. 2. Comparison of the differential recoil spectrum for WIMP-nucleon (black) $\mathcal{F}_+^M$ versus WIMP-pion interactions (red) $\mathcal{F}_\pi$. Exemplarily shown are WIMP masses of 30 GeV/c^2 (full line) and 200 GeV/c^2 (dashed line) for the most abundant isotope ^{132}Xe. The cross section in both cases is set to 10^{-46} cm^2 for illustration. The gray band shows the energy range for the XENON1T SI search. The inset compares the spectral shapes in this region.

$$\frac{dR}{dE_r} = \frac{2\rho_0\sigma_{\chi\pi}^{\text{scalar}}}{m_\chi\mu_\pi^2} \times |\mathcal{F}_\pi(q^2)|^2 \times \int_{v_{\min}(E_r)}^{\infty}\frac{f(\mathbf{v},t)}{v}d^3v, \tag{7}$$

where ρ_0 is the local dark matter density, $f(\mathbf{v},t)$ is its time-dependent velocity distribution truncated at escape velocity, and $v_{\min}$ is the minimal WIMP velocity possible for a given recoil energy and detector threshold. The main effect of the transition from the SI to the scalar WIMP-pion coupling concerns the form factor, where $\mathcal{F}_+^M(q^2)$ is replaced by $\mathcal{F}_\pi(q^2)$ [38,42]. Notably, the minimal velocity remains unchanged as the WIMP is still scattering off the entire xenon nucleus. A comparison to the standard expression (see Ref. [59]) shows that, as only the form factor influences the shape of the resulting spectrum, both provide a falling featureless exponential. A comparison of the differential recoil spectra of the WIMP-nucleon and the WIMP-pion scattering is shown in Fig. 2. Because of the similarity in shape, the same energy search window can be used for evaluating the WIMP-pion signal model as in the standard analysis [5]. For an attempt to discriminate between SI and WIMP-pion interactions, see Ref. [46].

Experiment.—To constrain the scalar WIMP-pion coupling, we use data from the XENON1T experiment [60]. This data reanalysis is part of the continued use and exploration of the XENON1T 1 t yr dataset. Parallel nuclear recoil (NR)

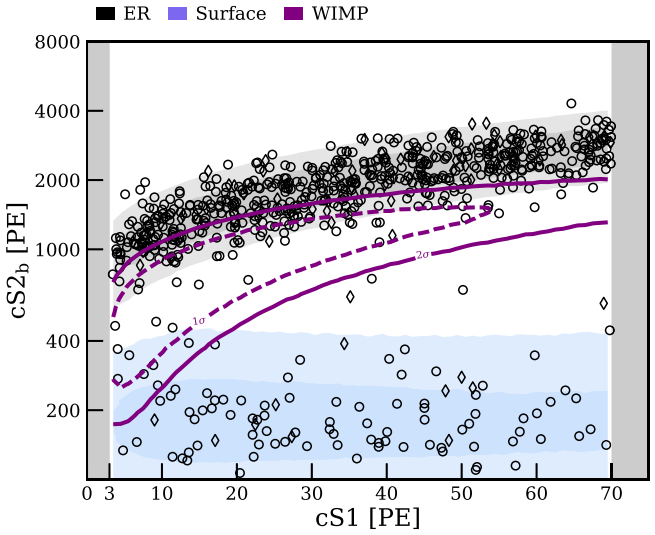

FIG. 3. XENON1T SR0 + SR1 data (black circles and diamonds, respectively, for each period), projected from the three-dimensional analysis space on the primary and secondary scintillation signal, $cS1$ and $cS2_b$, in units of photoelectrons (PEs). 1σ and 2σ containment regions for the WIMP-pion signal model for a 200 GeV/c^2 WIMP (purple contours), the electronic recoil background (gray bands), and surface background (blue bands) are shown.

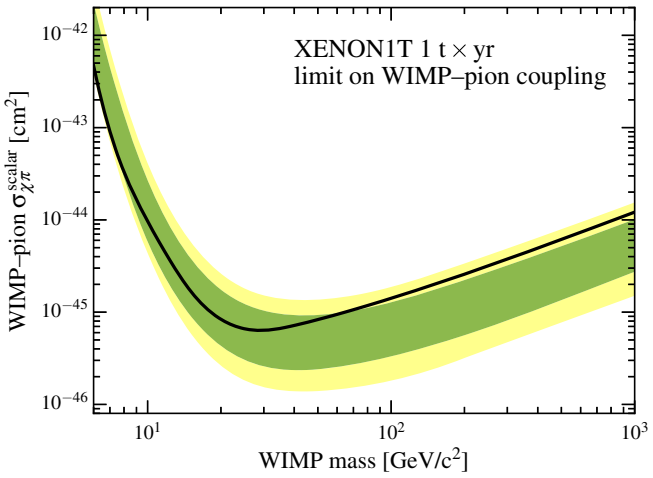

FIG. 4. 90% confidence level upper limit of the WIMP-pion coupling as a function of WIMP mass for the 1 t yr exposure of XENON1T data. Bands show the 1σ (green) and 2σ (yellow) quantiles of the expected no-signal distribution of upper limits.

searches are also under way (see Refs. [15,21] for XENON100 analyses beyond the SI channel). We use the same dataset and modeling as the SI analysis, except for the signal model, which is replaced by the recoil spectrum in Eq. (7). The following section gives a brief overview of the XENON1T detector and analysis procedure.

XENON1T is the world's largest dual-phase xenon TPC, shielded by rock overburden at a water equivalent depth of 3600 m at the Laboratori Nazionali del Gran Sasso. An active muon veto water tank [60] and an inactive layer of liquid xenon surround the cylindrical TPC. The 2.0 t target mass of liquid xenon with a gaseous xenon gap at the top is read out by two photomultiplier tube (PMT) arrays, located at the top and bottom of the detector. Energy deposition within the liquid xenon may produce scintillation photons and ionization electrons. Photons are directly registered as the first signal ($S1$) by the PMTs, while the electrons drift upward in an externally applied field $\mathcal{O}(100\mathrm{V/cm})$ to the liquid-gas interface. A strong electric field $\mathcal{O}(10\ \mathrm{kV/cm})$ extracts the electrons into the gas and accelerates them, leading to proportional scintillation in the gaseous phase and thus a secondary light signal ($S2$). The ratio between the two signals ($S2/S1$) allows one to distinguish statistically between NRs from neutrons and WIMPs, and electronic recoils (ERs) from γ and β particles. The measured $S1$ and $S2$ signals are compensated for the spatially inhomogeneous detector response, yielding the corrected analysis variables, $cS1$ and $cS2_b$, with the latter measured with the bottom PMT array. The time between the prompt $S1$ signal and the $S2$ signal measures the depth (z coordinate) of the interaction, while the transversal (x, y) position is reconstructed from the $S2$ pattern observed by the top PMT array, corrected for a small transverse drift field component. With a three-dimensional position reconstruction of events, the analysis can exclude large background populations at the detector edges by selecting an analysis volume. Motivated by the similarity of WIMP-pion and SI recoil spectra, the event selection criteria are the same as in Ref. [5]. The dark matter data are divided into SR0 [61], with 32.1 days live time, and SR1, with 246.7 days. Both the XENON1T SI analysis [5] and this search use the combined SR0 + SR1 dataset.

The signal distribution in $cS1$ and $cS2_b$ is derived by convolving the recoil spectrum in Eq. (7) with the detector NR response, calibrated with a deuterium-deuterium neutron generator [62] and an americium-241-beryllium neutron source. Background distributions for ERs, radiogenic and cosmogenic neutrons, coherent elastic neutrino-nucleus scatters (CEνNS), accidental coincidence of $S1$ and $S2$ signals (AC), and events originating from the detector surfaces are retained from the SI analysis. Figure 3 shows the combined dataset, as well as contours for the signal distribution due to a 200 GeV/c^2 WIMP, illustrating how a potential signal is separated in the $cS1$-$cS2_b$ plane from ER and surface background events.

Discovery significances and confidence intervals for the WIMP-pion interaction cross section are calculated using the profile likelihood ratio method. The combined likelihood includes extended unbinned likelihood terms for the SR0 and SR1 datasets, using signal and background models in the three-dimensional analysis space ($cS1$, $cS2_b$, radius), as well as a core volume with a lower neutron rate [5]. The full likelihood also includes additional terms for the ER calibration model fit and ancillary measurements of background rates. The discovery significance is expressed as the

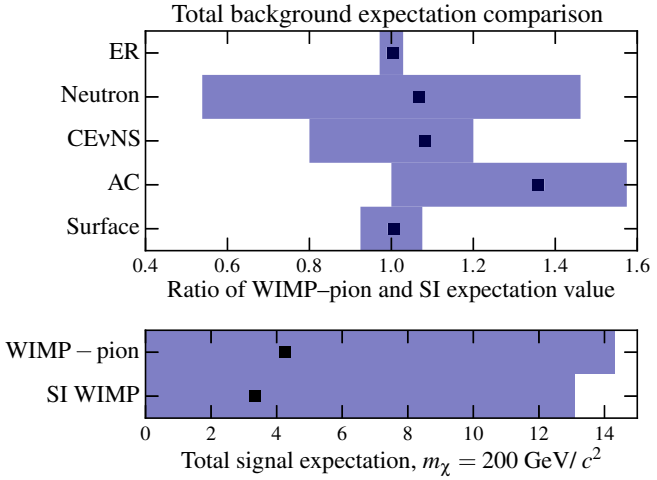

FIG. 5. Comparison of the WIMP-pion and standard SI WIMP maximum likelihood estimates (MLEs) of background and signal expectation values. The upper panel shows the ratio MLE expectation values for the present and the SI analyses. Blue bands show the 1σ confidence bands reported from the SI analysis. The lower panel shows the expected number of signal events for the WIMP-pion and the SI WIMP search [5] with squares indicating the MLE and the bands the 90% upper limits for the analyses.

local p value of the observed log-likelihood ratio between the best fit and no-signal models. The null distribution of this parameter is computed for each signal model (WIMP mass) using repeated realizations of the background-only model, since the low signal expectation values preclude the application of asymptotic results. Confidence intervals, both upper limits and two-sided intervals, are constructed based on a variant of the Feldman-Cousins [63] method using the profile likelihood ratio in the construction of the Neyman band [64]. This unified construction avoids undercoverage that can occur when an experiment switches between separate constructions for upper limits and two-sided intervals. The XENON1T experiment places a 3σ discovery significance threshold for reporting a two-sided interval.

Result and conclusions.—No significant signal-like excess is found in our analysis. The lowest local discovery p value is 0.14, observed for the high mass range above ~ 200 GeV$/c^2$. The 90% confidence level upper limit on the scalar WIMP-pion cross section, shown in Fig. 4, has a minimum of 6.4×10^{-46} cm^2 for a 30 GeV$/c^2$ WIMP. The comparison to the SI analysis is quantified in Fig. 5, in the upper panel for the ratio of the background expectations and in the lower one for the signal expectation, both computed for a 200 GeV$/c^2$ WIMP. No background component shows a significant deviation from the SI fit. The upper limits are within 8% in terms of signal expectation value, reflecting the comparable signal recoil energy spectra shown in Fig. 2. The difference in upper limit cross sections is therefore driven primarily by the different expectation values for the two interactions at the same cross section.

Summarizing, we have presented limits on the scalar WIMP-pion interaction, where the WIMP scatters off virtual pions in a nucleus via an underlying scalar WIMP-quark operator. The corresponding nuclear response for this interaction is coherently enhanced, similar to SI scattering, leading to the hierarchy given in Eq. (6). In analogy to standard SI and SD limits, the result can be represented in terms of a single-particle cross section. We have performed the first search for this interaction with 1 t yr of XENON1T data, using the XENON1T detector response, background models, and likelihood. We find no excess and set an upper limit on the scalar WIMP-pion cross section with a minimum at 6.4×10^{-46} cm^2 for a 30 GeV$/c^2$ WIMP (at 90% confidence level). Our analysis quantifies for the first time the effect of coherent two-body currents in direct-detection searches for dark matter, paving the way for future comprehensive studies of WIMP-nucleus interactions beyond SI and SD scattering.

The XENON collaboration gratefully acknowledges support from the National Science Foundation, Swiss National Science Foundation, German Ministry for Education and Research, Max Planck Gesellschaft, Deutsche Forschungsgemeinschaft, Netherlands Organisation for Scientific Research (NWO), Netherlands eScience Center (NLeSC) with the support of the SURF Cooperative, Weizmann Institute of Science, Israeli Centers of Research Excellence (I-CORE), Pazy-Vatat, Initial Training Network Invisibles (Marie Curie Actions, PITNGA-2011-289442), Fundacao para a Ciencia e a Tecnologia, Region des Pays de la Loire, Knut and Alice Wallenberg Foundation, Kavli Foundation, Abeloe Fellowship, and Istituto Nazionale di Fisica Nucleare. Data processing is performed using infrastructures from the Open Science Grid and European Grid Initiative. We are grateful to Laboratori Nazionali del Gran Sasso for hosting and supporting the XENON project. The work of M. H., P. K., J. M., and A. S. was supported by the U.S. DOE (Grant No. DE-FG02-00ER41132), the ERC (Grant No. 307986 STRONGINT), the Deutsche Forschungsgemeinschaft through SFB 1245 (Project No. 279384907), the Max-Planck Society, the Japanese Society for the Promotion of Science KAKENHI (Grant No. 18K03639), MEXT as "Priority Issue on Post-K computer" (Elucidation of the fundamental laws and evolution of the universe), JICFuS, and the CNS-RIKEN joint project for large-scale nuclear structure calculations.

*a.fieguth@uni-muenster.de
†Also at Albert Einstein Center for Fundamental Physics, University of Bern, Bern, Switzerland.
‡Also at Kobayashi-Maskawa Institute, Nagoya University, Nagoya, Japan.

[§]Also at Coimbra Polytechnic-ISEC, Coimbra, Portugal.
[¶]knut.mora@fysik.su.se
[**]xenon@lngs.infn.it
[††]mhofer@uw.edu

[1] G. Bertone, D. Hooper, and J. Silk, Phys. Rep. **405**, 279 (2005).
[2] L. Roszkowski, E. M. Sessolo, and S. Trojanowski, Rep. Prog. Phys. **81**, 066201 (2018).
[3] T. Marrodán Undagoitia and L. Rauch, J. Phys. G **43**, 013001 (2016).
[4] L. Baudis, J. Phys. G **43**, 044001 (2016).
[5] E. Aprile *et al.* (XENON Collaboration), Phys. Rev. Lett. **121**, 111302 (2018).
[6] G. Angloher *et al.* (CRESST Collaboration), Eur. Phys. J. C **76**, 25 (2016).
[7] E. Armengaud *et al.* (EDELWEISS Collaboration), J. Cosmol. Astropart. Phys. 05 (2016) 019.
[8] D. S. Akerib *et al.* (LUX Collaboration), Phys. Rev. Lett. **118**, 021303 (2017).
[9] C. Amole *et al.* (PICO Collaboration), Phys. Rev. Lett. **118**, 251301 (2017).
[10] P. A. Amaudruz *et al.* (DEAP-3600 Collaboration), Phys. Rev. Lett. **121**, 071801 (2018).
[11] X. Cui *et al.* (PandaX-II Collaboration), Phys. Rev. Lett. **119**, 181302 (2017).
[12] R. Agnese *et al.* (SuperCDMS Collaboration), Phys. Rev. Lett. **120**, 061802 (2018).
[13] P. Agnes *et al.* (DarkSide Collaboration), Phys. Rev. Lett. **121**, 081307 (2018).
[14] K. Abe *et al.* (XMASS Collaboration), Phys. Lett. B **789**, 45 (2019).
[15] E. Aprile *et al.* (XENON100 Collaboration), Phys. Rev. Lett. **111**, 021301 (2013).
[16] H. Uchida *et al.* (XMASS-I Collaboration), Prog. Theor. Exp. Phys. **2014**, 063C01 (2014).
[17] E. Aprile *et al.* (XENON100 Collaboration), Phys. Rev. D **94**, 122001 (2016).
[18] C. Fu *et al.* (PandaX-II Collaboration), Phys. Rev. Lett. **118**, 071301 (2017); **120**, 049902(E) (2018).
[19] D. S. Akerib *et al.* (LUX Collaboration), Phys. Rev. Lett. **118**, 251302 (2017).
[20] K. Schneck *et al.* (SuperCDMS Collaboration), Phys. Rev. D **91**, 092004 (2015).
[21] E. Aprile *et al.* (XENON Collaboration), Phys. Rev. D **96**, 042004 (2017).
[22] J. Xia *et al.* (PandaX-II Collaboration), arXiv:1807.01936.
[23] G. Angloher *et al.* (CRESST Collaboration), Eur. Phys. J. C **79**, 43 (2019).
[24] G. Angloher *et al.* (CRESST Collaboration), Phys. Rev. Lett. **117**, 021303 (2016).
[25] J. Fan, M. Reece, and L. T. Wang, J. Cosmol. Astropart. Phys. 11 (2010) 042.
[26] A. L. Fitzpatrick, W. Haxton, E. Katz, N. Lubbers, and Y. Xu, J. Cosmol. Astropart. Phys. 02 (2013) 004.
[27] N. Anand, A. L. Fitzpatrick, and W. C. Haxton, Phys. Rev. C **89**, 065501 (2014).
[28] E. Epelbaum, H.-W. Hammer, and U.-G. Meißner, Rev. Mod. Phys. **81**, 1773 (2009).
[29] R. Machleidt and D. R. Entem, Phys. Rep. **503**, 1 (2011).
[30] H.-W. Hammer, A. Nogga, and A. Schwenk, Rev. Mod. Phys. **85**, 197 (2013).
[31] S. Bacca and S. Pastore, J. Phys. G **41**, 123002 (2014).
[32] J. Menéndez, D. Gazit, and A. Schwenk, Phys. Rev. D **86**, 103511 (2012).
[33] P. Klos, J. Menéndez, D. Gazit, and A. Schwenk, Phys. Rev. D **88**, 083516 (2013); **89**, 029901(E) (2014).
[34] L. Baudis, G. Kessler, P. Klos, R. F. Lang, J. Menéndez, S. Reichard, and A. Schwenk, Phys. Rev. D **88**, 115014 (2013).
[35] V. Cirigliano, M. L. Graesser, and G. Ovanesyan, J. High Energy Phys. 10 (2012) 25.
[36] V. Cirigliano, M. L. Graesser, G. Ovanesyan, and I. M. Shoemaker, Phys. Lett. B **739**, 293 (2014).
[37] M. Hoferichter, P. Klos, and A. Schwenk, Phys. Lett. B **746**, 410 (2015).
[38] M. Hoferichter, P. Klos, J. Menéndez, and A. Schwenk, Phys. Rev. D **94**, 063505 (2016).
[39] C. Körber, A. Nogga, and J. de Vries, Phys. Rev. C **96**, 035805 (2017).
[40] M. Hoferichter, P. Klos, J. Menéndez, and A. Schwenk, Phys. Rev. Lett. **119**, 181803 (2017).
[41] L. Andreoli, V. Cirigliano, S. Gandolfi, and F. Pederiva, arXiv:1811.01843.
[42] M. Hoferichter, P. Klos, J. Menéndez, and A. Schwenk, arXiv:1812.05617.
[43] J. Goodman, M. Ibe, A. Rajaraman, W. Shepherd, T. M. P. Tait, and H. B. Yu, Phys. Rev. D **82**, 116010 (2010).
[44] J. Engel, S. Pittel, and P. Vogel, Int. J. Mod. Phys. E **01**, 1 (1992).
[45] M. T. Ressell, M. B. Aufderheide, S. D. Bloom, K. Griest, G. J. Mathews, and D. A. Resler, Phys. Rev. D **48**, 5519 (1993).
[46] A. Fieguth, M. Hoferichter, P. Klos, J. Menéndez, A. Schwenk, and C. Weinheimer, Phys. Rev. D **97**, 103532 (2018).
[47] R. H. Helm, Phys. Rev. **104**, 1466 (1956).
[48] L. Vietze, P. Klos, J. Menéndez, W. C. Haxton, and A. Schwenk, Phys. Rev. D **91**, 043520 (2015).
[49] M. Freytsis and Z. Ligeti, Phys. Rev. D **83**, 115009 (2011).
[50] A. Kurylov and M. Kamionkowski, Phys. Rev. D **69**, 063503 (2004).
[51] F. Giuliani, Phys. Rev. Lett. **95**, 101301 (2005).
[52] S. Chang, J. Liu, A. Pierce, N. Weiner, and I. Yavin, J. Cosmol. Astropart. Phys. 08 (2010) 018.
[53] J. L. Feng, J. Kumar, D. Marfatia, and D. Sanford, Phys. Lett. B **703**, 124 (2011).
[54] D. Gazit, S. Quaglioni, and P. Navrátil, Phys. Rev. Lett. **103**, 102502 (2009).**122**, 029901(E) (2019).
[55] R. J. Hill and M. P. Solon, Phys. Rev. Lett. **112**, 211602 (2014).
[56] C. Cheung, L. J. Hall, D. Pinner, and J. T. Ruderman, J. High Energy Phys. 05 (2013) 100.
[57] P. Huang and C. E. M. Wagner, Phys. Rev. D **90**, 015018 (2014).
[58] A. Crivellin, M. Hoferichter, M. Procura, and L. C. Tunstall, J. High Energy Phys. 07 (2015) 129.
[59] J. D. Lewin and P. F. Smith, Astropart. Phys. **6**, 87 (1996).
[60] E. Aprile *et al.* (XENON Collaboration), Eur. Phys. J. C **77**, 881 (2017).
[61] E. Aprile *et al.* (XENON Collaboration), Phys. Rev. Lett. **119**, 181301 (2017).

[62] R. F. Lang, J. Pienaar, E. Hogenbirk, D. Masson, R. Nolte, A. Zimbal, S. Röttger, M. L. Benabderrahmane, and G. Bruno, Nucl. Instrum. Methods Phys. Res., Sect. A **879**, 31 (2018).

[63] G. J. Feldman and R. D. Cousins, Phys. Rev. D **57**, 3873 (1998).

[64] M. Tanabashi *et al.* (Particle Data Group), Phys. Rev. D **98**, 030001 (2018).